Docking and Mutagenesis Studies Lead to Improved Inhibitor Development of ML355 for Human Platelet 12-lipoxygenase.

Wan-Chen Tsai[1], Ansari M. Aleem[1†], Jennyfer Tena [1¢], Mirella Rivera-Velazquez[1], Harman Singh Brah[2], Sarvind Tripathi[1], Melinee D'silva[3], Jerry L. Nadler[3], Chakrapani Kalyanaraman[2], Mathew P. Jacobson[2], Theodore Holman[1]*

[1]Department of Chemistry and Biochemistry, University of California Santa Cruz, Santa Cruz, CA 95064, United States

[2]Department of Pharmaceutical Chemistry, School of Pharmacy, University of California San Francisco, San Francisco, CA 94143, United States

[3]Department of Medicine and Pharmacology, New York Medical College, Valhalla, NY 10595, United States

***Corresponding Author:** Tel.: +1 831 459 5884; fax: +1 831 459 2935.
E-mail address: holman@ucsc.edu

[†]Current Address: A. B. Hancock, Jr. Memorial Laboratory for Cancer Research, Department of Biochemistry, Vanderbilt University, Nashville, TN 37232, USA.
[¢]Current Address: Department of Chemistry, University of California Davis, Davis, CA 95616, USA.

Abstract

Human platelet 12-(S)-Lipoxygenase (12-LOX) is a fatty acid metabolizing oxygenase that plays an important role in platelet activation and cardiometabolic disease. **ML355** is a specific 12-LOX inhibitor that has been shown to decrease thrombosis without prolonging hemostasis and protect human pancreatic islets from inflammatory injury. It has an amenable drug-like scaffold with nM potency and encouraging ADME and PK profiles, but its binding mode to the active site of 12-LOX remains unclear. In the current work, we combined computational modeling and experimental mutagenesis to propose a model in which **ML355** conforms to the "U" shape of the 12-LOX active site, with the phenyl linker region wrapping around L407. The benzothiazole of **ML355** extends into the bottom of the active site cavity, pointing towards residues A417 and V418. However, reducing the active site depth alone did not affect **ML355** potency. In order to lower the potency of **ML355**, the cavity needed to be reduced in both length and width. In addition, H596 appears to position **ML355** in the active site through an interaction with the p-methoxy catechol moiety of **ML355**. Combined, this binding model suggested that the benzothiazole of **ML355** could be enlarged. Therefore, a naphthyl-benzothiazole derivative of **ML355**, **Lox12Slug001**, was synthesized and shown to have 7.2-fold greater potency than **ML355**. This greater potency is proposed to be due to additional van der Waals interactions and pi-pi stacking with F414 and F352. **Lox12Slug001** was also shown to be highly selective against 12-LOX relative to the other LOX isozymes and more importantly, it showed activity in rescuing human islets exposed to inflammatory cytokines with comparable potency to **ML355**. Further studies are currently being pursued to derivatize **ML355** in order to optimize the additional space in the active site, while maintaining acceptable drug-like properties.

Key words: Human platelets, 12-Lipoxygenase, ML355, drug discovery, optimization, cardiovascular diseases, diabetes, mutagenesis, computational modeling.

1. Introduction

Human Platelet-type 12-(S)-lipoxygenase (12-LOX, ALOX12) is a non-heme iron-containing oxygenase that catalyzes the regio- and stereo-specific addition of molecular oxygen to polyunsaturated fatty acids (PUFA).[1] 12-LOX belongs to a family of enzymes that also include 5-LOX (ALOX5) and 15-LOX (ALOX15 and ALOX15b), which oxygenate arachidonic acid (AA) at their corresponding carbon positions. The hydroperoxyeicosatetraenoic acid (HPETE) product is subsequently reduced by cellular peroxidases to form the hydroxyeicosatetraenoic acid (HETE), which in the case of 12-LOX is 12-(S)-HETE.[2]

Although 12-LOX is highly expressed in platelets (~14,000 molecules per platelet), it is also expressed in some hematopoietic, solid tumors and pancreatic islets.[3-5] To date, 12-LOX is the only LOX isoform identified to be present in platelets, and its activity is crucial for a number of platelet functions, including granule secretion, platelet aggregation, and normal adhesion through specific agonist-mediated pathways, such as collagen and the thrombin receptor, PAR4.[6] Normal platelet activation plays a central role in the regulation of hemostasis, but uncontrolled activation can lead to pathologic thrombotic events, such as ischemic coronary heart disease.[7-13] Although currently approved antiplatelet drugs, such as Ticlopidine , Clopidogrel, Prasugrel, Abciximab, Eptifibatide, Tirofiban and Dipyridamole have significantly decreased the morbidity and mortality of ischemic heart disease, their efficacy is limited by the subsequent increased risk of severe bleeding.[14] This limitation has motivated the development of new approaches for limiting platelet activation, and a number of new platelet targets are currently being investigated for their potential to limit clot formation, such as thrombin receptor (PAR1), αIIbβ3 and GPVI antagonists (reviewed by Holinstat and coworkers).[14] In addition to these new platelet targets, we propose that since 12-LOX is a key pro-thrombotic enzyme within the platelet, it may also be an effective approach to anti-platelet therapy.[6, 15, 16]

The relationship of the mouse form of ALOX12 to the development of diabetes has been validated in genetic deletion studies, where global deletion of the gene led to significant protection (>98%) from diabetes development in both the streptozotocin (STZ) and spontaneous non-obese diabetic (NOD) mouse models (reviewed in [5]). The 12-LOX inhibitor, **ML355**, has facilitated dissection of the contribution of these pathways to inflammation-mediated beta cell dysfunction. Exposure of beta cell lines and primary islets to pro-inflammatory cytokines (PIC; TNF-α, IL-1β, IFN-γ) results in compromised beta cell function and survival. The effects of PICs can be reproduced with direct addition of 12-HETE. This implied role for 12-LOX activation as a mediator of beta cell dysfunction was validated with the use of **ML355** in human islets. The markers of beta cell function and survival were preserved in the presence of PICs and in islets from people with Type-2 diabetes. Such a strategic approach would slow the progression of diabetes as a mono-therapy, or reverse diabetes as a combinatorial therapeutic approach when coupled with an islet regeneration strategy. This could be utilized in either endogenous beta cell stimulation or exogenous repopulation (cell transplantation/encapsulation/xenotransplantation etc.). 12-LOX is also expressed in central adipose tissue from human samples of obese individuals, which could reflect opportunities to target 12-LOX to reduce metabolic and vascular complications due to obesity and diabetes.

Few potent and selective 12-LOX inhibitors have been reported in the literature.[5] Initially, selective 12-LOX inhibitors were found in natural sources, such as hinokitiol,[17] bromophenols[18] and isoflavanones,[19] but they had liabilities for further development into drugs. High-throughput screening produced a number of selective inhibitors,[20, 21] including N-benzo[d]thiazol-2-yl)-4((2-hydroxy-3 methoxybenzyl)-amino) benzenesulfonamide (**ML355**).[22] **ML355** is a non-reductive, reversible, mixed-type 12-LOX inhibitor with nM potency and excellent selectivity over related enzymes, including 5-LOX, 15-LOX-1, 15-LOX-2, COX1, and COX2. **ML355** also has encouraging *in vitro* absorption, distribution, metabolism and excretion (ADME) and *in vivo* pharmacokinetic (PK) profiles. *In vitro* studies have shown that **ML355** reduces platelet aggregation in response to low dose platelet activators[23] and oral administration of **ML355** in mice limits thrombosis formation without significant prolongation of hemostasis.[24] **ML355** also inhibits platelet activation mediated by the immune receptor, FcγRIIa,[23] which is required for immune-mediated thrombocytopenia, such as heparin-induced thrombocytopenia (HIT). **ML355** has been used to delineate the role of 12-LOX in hemostasis,[23] and improves human islet function after cytokine treatment in vitro.[5, 25] These studies indicate that **ML355** could represent a viable approach to decrease platelet reactivity following vascular insult or injury, while minimizing the increased risk of bleeding that is concomitant with antiplatelet therapy.[26] Unfortunately, no structure of **ML355** bound to 12-LOX has been published yet, therefore, we have employed site-directed mutagenesis and molecular modeling to elucidate a binding model of **ML355** to its target 12-LOX, and utilize that information to guide the synthesis of a novel 12-LOX inhibitor. This novel inhibitor has 7.2-fold improved potency and equivalent cellular activity in human islets relative to **ML355** and indicates possible avenues for improved analogues to **ML355**.

2. Experimental procedures

2.1. Chemicals

Fatty acids used in this study were purchased from Nu Chek Prep, Inc. (MN, USA). All other solvents and chemicals were reagent grade or better and were used as purchased without further purification.

2.2. Molecular modeling

A homology model of the human platelet 12-LOX catalytic domain (Uniprot accession P18054) was built based on the porcine leukocyte 12(S)-LOX structure (PDB ID: 3RDE, sequence identity 65%), using the software Prime (version 6.0 , Schrodinger Inc.). During homology modeling, the metal ion (Fe^{3+}), the iron coordinated hydroxide ion and the co-crystallized ligand, 3-{4-[(tridec-2-yn-1-yloxy) methyl] phenyl} propanoic acid, from the porcine 12(S)-LOX structure were retained. In the published structure, a water is shown coordinating the metal ion; for our modeling purposes, we assigned iron to the ferric (Fe^{3+}) oxidation state, with a coordinating hydroxide to mimic the catalytically-competent state and complete the octahedral symmetry [27]. The human 12-LOX model was subsequently energy minimized using Protein

Preparation Wizard (Schrodinger Inc). During this step, hydrogen atoms were added and optimized to make better hydrogen bonding interactions, and all heavy atoms were energy minimized with a restraint such that they did not move beyond 0.3 Å from their starting positions. The structure of **ML355** was prepared using Edit/Build panel of Maestro software (version 12.4, Schrodinger Inc.) and energy minimized using LigPrep software (Schrodinger Software Suite 2020-2).

Initially, we docked **ML355** to the wild-type (wt) protein using the docking software Glide (version 8.7, Schrodinger Inc.), consisting of grid preparation and virtual screening. We used the coordinates of the co-crystallized ligand from the porcine 12-LOX homolog to define the grid center. Following grid preparation, we docked **ML355** to the 12-LOX active site using standard-precision (SP) scoring function. Only the ligand was treated flexibly during docking.

Starting from the wt protein structural model, we made each mutant protein using the *Mutate Residue* option in the Build panel of the Maestro software. After making the virtual mutation, we predicted sidechain conformation of the mutated residue using the software Prime (version 6.0, Schrodinger Inc.). During the sidechain prediction step, except for the metal and the hydroxide ions, all the other modeled compounds were removed from the active site. The protein was held rigid and only the conformation of the mutated residue was optimized. We then used the coordinates of **ML355** docked to the wt protein to define the docking grid center for each mutant protein. After the grid preparation step, **ML355** was docked to the mutant proteins using Glide with the SP scoring function.

2.3. Site-directed mutagenesis

Based on the **ML355** binding mode predicted by the modeling, we selected all residues within 5 Å of any atom of **ML355** for experimental mutagenesis. The selected residues were replaced with amino acids with either bulkier or smaller side chains in order to determine what specific interactions play a role in inhibitor binding. The following mutations were made: F352L, I399L, I399M, E356A, E356K, L361M, R402L, A403S, L407A, L407G, I413A, F414L, A417I, V418M, A417I/V418M, Q547L, and L597M. The numbering refers to the UniProt accession number P18054 sequence, with the N-terminal methionine assigned as amino acid number one. The primers for all mutants were designed using the online QuikChange Primer Design tool (***http://www.genomics.agilent.com/primerDesignProgram.jsp***) from Agilent Technologies (CA, USA). The mutations were introduced by using the QuikChange®II XL site-directed mutagenesis kit from Agilent, following the instructions in the protocol provided. The mutations were confirmed by sequencing the 12-LOX insert in the pFastBac1 shuttle vector (Eurofins Genomics, KY, USA).

2.4. Protein expression and purification

The expression and purification of 12-LOX (UniProt entry P18054) and all mutants used in this study were performed as described previously[28]. Briefly, the wild type 12-LOX (wt-12-LOX) enzyme and its mutants were expressed as fusion proteins, with an N-terminal 6xHis tag, and were affinity purified by nickel-iminodiacetic acid agarose using FPLC (Biorad). For inhibitor selectivity, human 5-LOX (h5-LOX, UniProt entry P09917), human reticulocyte 15-LOX-1 (h15-LOX-1, UniProt entry P16050) and human epithelial 15-LOX-2 (h15-LOX-2, UniProt

entry O15296) were also isolated, as previously described.[19, 29, 30] The purity of all the proteins, except h5-LOX, was greater than 90% as determined by SDS-PAGE analysis. h5-LOX was an ammonium sulfate fraction due to the extensive loss of activity upon purification.[31]

2.5. Determination of iron content using ICP-MS

The iron content of wt12-LOX and the mutant enzymes that exhibited a significant change in their IC_{50} values was determined by a Thermo Element XR inductively-coupled plasma mass spectrometer (ICP-MS), using cobalt (EDTA) as an internal standard. Iron concentrations were compared with standardized iron solutions and all kinetic data were normalized to the iron content. The Bradford assay, with bovine serum albumin (BSA) as the protein standard, was used to determine the protein concentration.

2.6. Steady-state kinetics

The kinetic rates of wt12-LOX and mutant enzymes that exhibited more than 3.5-fold increase in the IC_{50} values were determined by monitoring the formation of the conjugated diene product, 12(S)-HpETE (ε = 25,000 $M^{-1}cm^{-1}$) at 234 nm, with a Perkin-Elmer Lambda 40 UV/Vis spectrophotometer. The reactions were initiated by adding the appropriate amount of enzyme to a 2 mL reaction mixture containing 1-20 μM AA, 25 mM HEPES buffer (pH 8.0), 0.01% Triton X-100, at 23°C, with constant stirring using a magnetic bar. Kinetic data were obtained by recording initial enzymatic rates at each substrate concentration and then fitting them to the Michaelis-Menten equation using KaleidaGraph (Synergy) to determine the k_{cat} and k_{cat}/K_M values.

2.7. UV-Vis-based IC_{50} assay for lipoxygenase isozymes

IC_{50} values of **ML355** and **Lox12Slug001** against 12-LOX and its mutants were determined in a similar manner as the steady state kinetic values. The percent inhibition was determined by comparing the enzyme rates of the control (DMSO solvent) and the inhibitor sample by following the formation of the conjugated diene product at 234 nm (ε = 25,000 $M^{-1}cm^{-1}$). The reactions were initiated by adding 200 nM 15-LOX-2, 30 nM 12-LOX, 40 nM 15-LOX-1, or approximately 100 - 300 nM (total protein) of 5-LOX ammonium sulfate fraction to a cuvette with 2 mL reaction buffer, constantly stirred using a magnetic stir bar at room temperature (22 ºC). Reaction buffers used for various LOX isozymes were as follows: 25 mM HEPES (pH 7.3), 0.3 mM $CaCl_2$, 0.1 mM EDTA, 0.2 mM ATP, 0.01% Triton X-100, 10 μM AA for the crude, ammonium sulfate precipitated 5-LOX; and 25 mM HEPES (pH 7.5), 0.01% Triton X-100, 10 μM AA for 15-LOX-2, 15-LOX-1, and 12-LOX. The substrate concentration was quantitatively determined by allowing the enzymatic reaction to go to completion in the presence of soybean LOX-1. IC_{50} values were obtained by determining the % inhibition, relative to solvent vehicle only, at various inhibitor concentrations. The data were then plotted against inhibitor concentration, followed by a hyperbolic saturation curve fit (assuming total enzyme concentration [E] << IC_{50}). It should be noted that all of the potent inhibitors displayed greater than 80% maximal inhibition, unless otherwise stated in the tables. All inhibitors were stored at −20 °C in DMSO.

2.8. Synthesis of 4-((2-hydroxy-3-methoxybenzyl)amino)-N-(naphtho[1,2-d]thiazol-2-yl)benzenesulfonamide (Lox12Slug001)

General Methods for Chemistry.

All air or moisture sensitive reactions were performed under positive pressure of nitrogen with oven-dried glassware. Chemical reagents and anhydrous solvents were obtained from commercial sources and used as-is. The analog for assay has purity greater than 95% and ^{1}H and ^{13}C NMR spectra were recorded on Bruker Avance III HD 500MHz NMR spectrometer.

General Synthetic Procedures. The synthesis of the **ML355** derivatives were achieved with the following steps (**Scheme 1**).

Step 1. To a stirred solution of naphtho[1,2-d]thiazol-2-amine (1eq.) in pyridine (6 eq.) was added N-acetylsulfanilyl chloride (1.1 eq.) in three equal parts. The reaction mixture was heated for 4 hrs at 100 °C and allowed to cool to room temperature. The reaction mixture was then allowed to sit at room temperature for 2 hrs, and afterwards was poured into EtOAc and 1N $HCl_{(aq.)}$ in a separation funnel. A white solid was formed in the EtOAc layer, which was collected by filtration, washed with cold ethanol, and dried under reduced pressure overnight to give the desired acetamide product (yield: 58 %).

Step 2. To a stirred solution of the acetamide product (1 eq.) in MeOH (2 mL) was added 4M HCl in dioxane (1.5 eq.). The reaction was heated for 2 hrs at 100 °C and then cooled to room temperature. The reaction mixture was then concentrated with a rotavap to get the white solid amine product (yield: 92%).

Step 3. The amine product (1 eq.) in anhydrous ethanol (1mmol of amine product in 5 mL) was added to TEA (2eq.) and stirred for 1 hr at room temperature. 2-hydroxy-3-methoxybenzaldehyde (1.2 eq.) was then added to the reaction mixture and refluxed overnight. The reaction mixture was then cooled to room temperature before sodium borohydride (3 eq.) was added and stirred for 2hrs. The reaction was quenched with MeOH and water until it stopped bubbling. The white solid was collected by filtration, washed with cold EtOH and then dried under vacuum. The crude solid was purified by RP-18 column chromatography (3 column volumes of 20% MeOH w/0.1% NH_4OH in water to wash out the impurity then elute out the product with 50% MeOH w/0.1% NH_4OH in water) to give the desired final product (yield: 28 %).

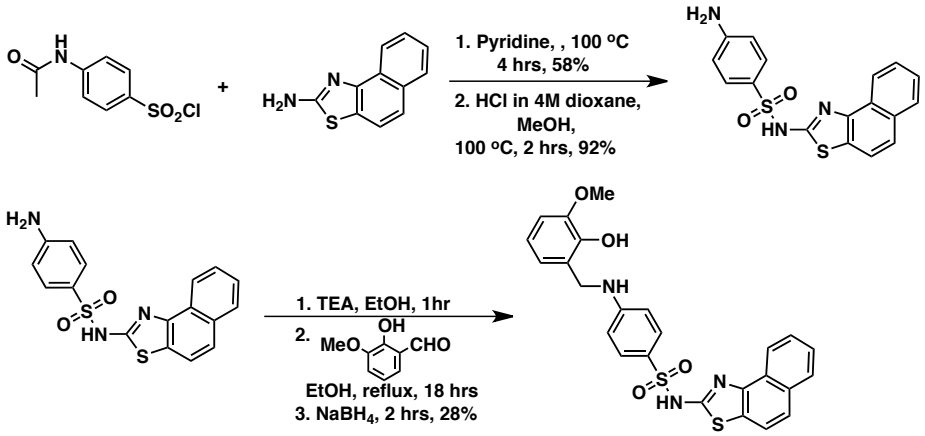

Scheme 1. Synthesis of 4-((2-hydroxy-3-methoxybenzyl)amino)-N-(naphtho[1,2-d]thiazol-2-yl)benzenesulfonamide (**Lox12Slug001**).

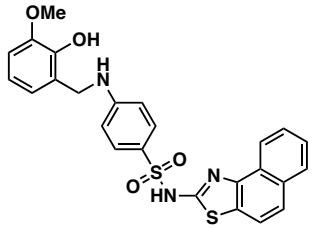

4-((2-hydroxy-3-methoxybenzyl)amino)-*N*-(naphtho[1,2-*d*]thiazol-2-yl)benzenesulfonamide
^{1}H NMR (500 MHz, DMSO-d_6) δ 8.69 (s, 1H), 8.34 (d, J = 5 Hz, 1H), 7.93 (s, 1H), 7.77 (s, 1H), 7.53 (d, J = 10 Hz, 4H), 6.81 (d, J = 10 Hz, 1H), 6.73 (d, J = 10 Hz, 1H), 6.66 (t, J = 5 Hz, 1H), 6.57 (d, J = 5 Hz, 2H), 4.21 (d, J = 10 Hz, 2H), 3.77 (s, 3H), Figure S1. ^{13}C NMR (500 MHz, DMSO-d_6) δ 147.1, 143.5, 131.3, 127.6, 127.5, 127.3, 125.6, 119.8, 119.1, 118.4, 110.3, 110.1, 55.6, 40.6, Figure S2.

2.9. Culture of Human Islets

Human islets from nondiabetic donors were received from the Integrated Islet Distribution Program or Prodo Laboratories (Aliso Viejo, CA) (**Table 1**). Characteristics of islets and donors are summarized in the below table. Islets were incubated in CMRL-1066 medium supplemented with 10% fetal bovine serum and 1% Pen-Strept overnight at 37°C in 5% CO_2 for recovery from shipment. On the next day, islets were transferred to CMRL-1066 supplemented with 5% fetal bovine serum and 1% Pen-Strept. A portion of the islets were randomly selected and incubated with a mixture of human PICs, 0.57 mmol/L tumor necrosis factor α, 5.9 mmol/L interferon-γ, and 0.29 mmol/L IL-1β (all from BD Biosciences, San Jose, CA) in the presence or absence of 1 μmol/L **Lox12Slug001**. The **Lox12Slug001** was added 30 minutes before the addition of pro-inflammatory cytokines (PIC)[25].

Table 1. Characteristics of Human Islet Donors

Sex	Age (y)	BMI (kg/m^2)	Cause of Death, A1c Value if Reported	Study Done	Source
F	60	44.4	Head Trauma	Nondiabetic donors	IIDP
F	53	32.5	Anoxic event, HbA1c 5.2%	Nondiabetic donors	Prodo

M	34	28.1	Head trauma	Nondiabetic donors	IIDP

2.10 Glucose Stimulated Insulin Secretion

Use of Krebs-Ringer buffer (KRB) for glucose-stimulated insulin secretion (GSIS) was previously published. For batch assays, islets treated with PIC in the presence or absence of **Lox12Slug001** (1 μM) for 24 hours were transferred to KRB without glucose and were incubated for 1 hour at 37°C in 5% CO_2 in the absence of PIC and **Lox12Slug001**. Thereafter, 50 islet equivalents (IEQs) per well were transferred to six-well plates filled with 1 mL of KRB containing 3 mmol/L or 18 mmol/L of glucose and were incubated for 1 hour at 37°C in 5% CO_2. Each condition was performed in triplicate. After incubation, supernatant was collected for determination of insulin secretion by human insulin enzyme-linked immunosorbent assay (Mercodia, Winston-Salem, NC) [25].

2.11 Statistics

Data are presented as mean ± standard error of the mean and were analyzed using Two-way Anova analysis of variance Sidak's multiple comparison test (Prism software, Irvine, CA) as indicated in each figure. $P < 0.05$ was considered significant.

3. Results and discussion

3.1 Computational Modeling of ML355 Interactions with wt12-LOX and its mutants.

ML355 is a potent/selective inhibitor of 12-LOX, however little is known regarding its specific molecular interactions in the active site of 12-LOX. In order to rectify this deficiency, a homology model of the 12-LOX catalytic domain was constructed and **ML355** was docked into the catalytic site. Our model predicted **ML355** to bind tightly in the active site with a standard-precision (SP) docking score of -10.37. The docking pose (**Figure 1**) shows the following interactions between **ML355** and 12-LOX: the amidine hydrogen forms a hydrogen bond with the backbone carbonyl oxygen of I399, the bridging aromatic ring forms a pi-stacking interaction with the metal-coordinated H365, the epsilon nitrogen of H596 is 3.6 Å from the oxygen atom of the hydroxyl group on the p-methoxy catechol moiety, **ML355** wraps around L407, and the **ML355** benzothiazole ring is buried in a hydrophobic pocket, whose base is defined by A417/V418 and whose sides are defined by the aromatic residues, F352 and F414. To test critical interactions predicted by this structural model, homology models were constructed of mutated proteins (**Table 2**). In parallel, the 12-LOX mutants were purified and their IC_{50} values determined to assess the validity of the docking model. Gratifyingly, the docking scores show a positive correlation with the experimental IC_{50} values (**Figure 2**), which lend support to our docking model of **ML355** in the 12-LOX active site.

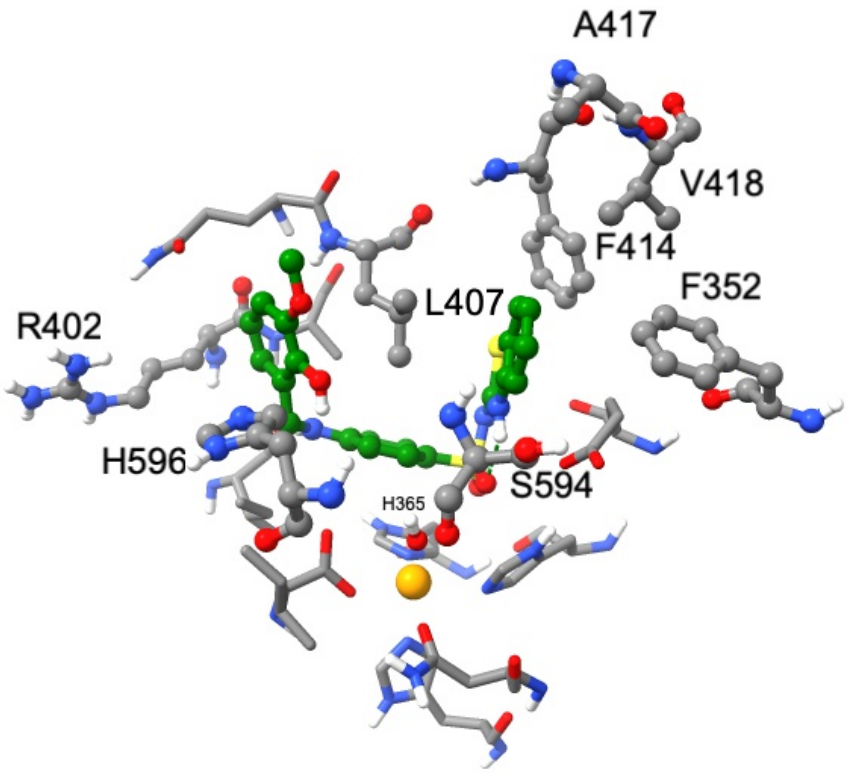

Figure 1. Predicted binding mode of **ML355** with wt12-LOX. Carbon atoms of **ML355** are shown in green, whereas carbon atoms of the protein are shown in gray. Nitrogen, oxygen, hydrogen and sulfur atoms are shown in blue, red, white and yellow colors respectively. Residues interacting with **ML355** and the metal ion are also shown. Residues that were mutated in this study are shown in ball-and-stick representation and labeled, whereas other residues are shown in stick representation. A hydroxide ion interacting with Fe^{3+} is also shown in ball-and-stick representation. Fe^{3+} ion is shown as an orange sphere. Hydrogen bonds are shown in cyan color.

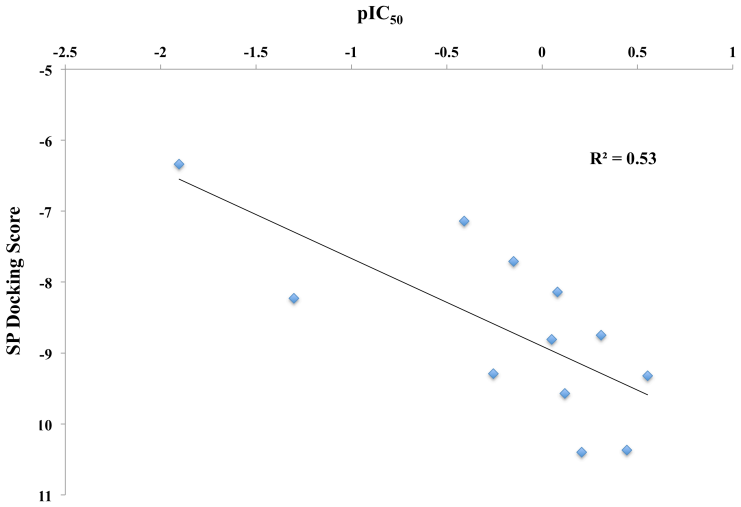

Figure 2. Correlation of pIC_{50} values of **ML355** against human 12-LOX mutants to the docking scores.

Enzyme	ML355 IC_{50} (μM)	SP Docking Score
wt12-LOX	0.36 ± 0.02	-10.4
R402L	0.28 ± 0.06	-9.32
H596L	1.8 ± 0.4	-9.29
L407A	1.4 ± 0.18	-7.71
L407G*	2.6 ± 0.86	-7.14
A417I	0.62 ± 0.08	-10.4
V418M	0.76 ± 0.07	-9.57
A417I/V418M	0.83 ± 0.2	-8.14
A417I/V418M/S594T	>20	-8.23
A417I/V418M/L407G	>80	-6.34
F414L	0.49 ± 0.03	-8.75
F352L	0.89 ± 0.08	-8.81

Table 2. ML355 IC_{50} values and the SP docking scores of the wt12-LOX and the mutant enzymes. *The high error for L407G is due to is low absolute activity.

3.2 Critical Role of L407 in ML355 Positioning

On the basis of the computational model of **ML355** in the active site, the importance of the bulky hydrophobic residue, L407, was investigated. The side chain of L407, along with I399, A403, L597, forms a narrow hydrophobic channel for the substrate. As shown in **Figure 1**, the phenyl ring linker of **ML355** fills the hydrophobic channel in the wt-12-LOX binding pose. Mutation of L407 to a smaller hydrophobic residue, such as Ala or Gly, greatly widens the hydrophobic channel, and is predicted to reduce favorable hydrophobic contacts with **ML355**, which in turn would affect **ML355** potency (**Figure 3**). In fact, L407A caused a 3.9-fold decrease in inhibitory potency compared to wt12-LOX, 1.4 ± 0.18 μM and 0.36 ± 0.02 μM, respectively. The inhibitory potency decreased even more when the cavity was made larger with the L407G mutant enzyme, with a 7.2-fold decrease in IC_{50} relative to wt-12-LOX (2.6 ± 0.9 μM).

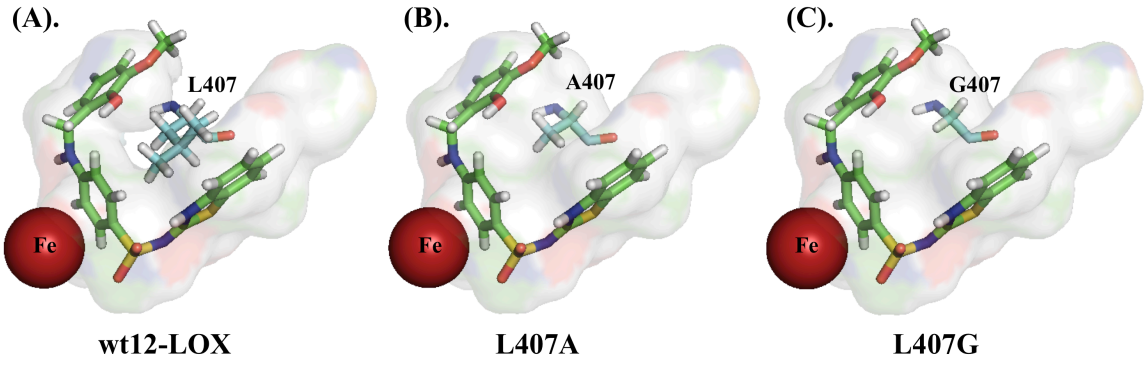

Figure 3. Relative cavity shapes and sizes of **ML355** binding in the active site of **(A).** wt12-LOX **(B).** L407A and **(C).** L407G

3.3 Role of A417, V418 and S594 in ML355 binding and the development of a more potent ML355 derivative, Lox12Slug001

Residues A417 and V418 (**Figure 1**), known as the Sloane determinants, form the bottom of the active site cavity and play a major role in the substrate positional specificity of 12-LOX [32]. However, our **ML355** docking model did not indicate a structural interaction between these two residues and the inhibitor (**Figure 4**). The benzothiazole of **ML355** was positioned 6.9Å away from A417 and 4.2Å away from V418. Therefore, the mutants A417I, V418M, and A417I/V418M were tested to determine if the decreased depth of the active site would affect **ML355** potency. As predicted by our docking model, mutating these two residues to bulkier amino acids showed only a modest change of the IC_{50} value compared to the wt-12LOX, with only a 2.3-fold decrease in potency in the double mutant (A417I/V418M) (**Figure 4, Table 2**).

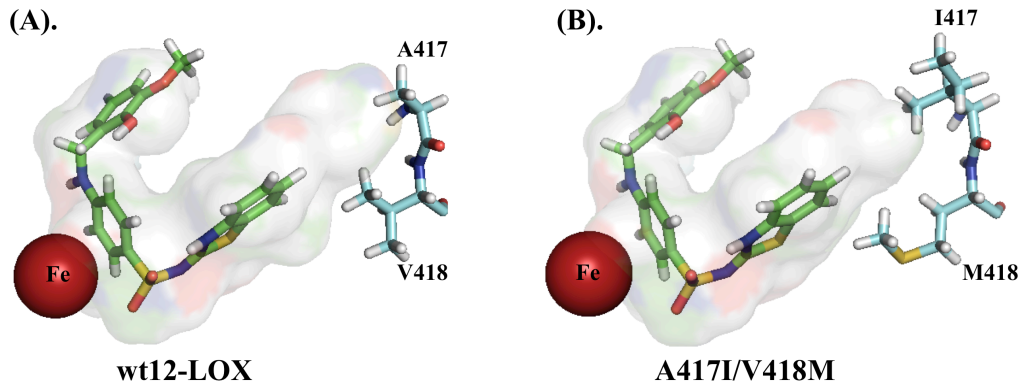

Figure 4. Relative cavity sizes of **ML355** binding in the active site of **(A).** wt12-LOX and **(B).** A417I/V418M (Sloane determinants)

This result indicated that bulkier substituents on the benzothiazole ring of **ML355** could be tolerated and possibly increase the **ML355** derivative potency by increased hydrophobic interactions in the deepest portion of the active site. Therefore, the **ML355** derivative, 4-((2-hydroxy-3-methoxybenzyl)amino)-N-(naphtho[1,2-d]thiazol-2-yl)benzenesulfonamide (**Lox12Slug001**) was designed and docked to the 12-LOX active site and found to have a favorable binding score of -11.40 (**Figure 5**). The molecule was subsequently synthesized

(**Lox12Slug001**, **Scheme 1**) and its potency was observed to increase by 7.2-fold (IC_{50} = 0.050 ± 0.02 uM) (**Table 3**) against the wt12-LOX. **Lox12Slug001** also showed high selectivity against h5-LOX, h15-LOX-1 and h15-LOX-2 (**Table 4**). In total, these data support our binding model for **ML355** docking to the active site of 12-LOX and indicates opportunities for further increases in potency.

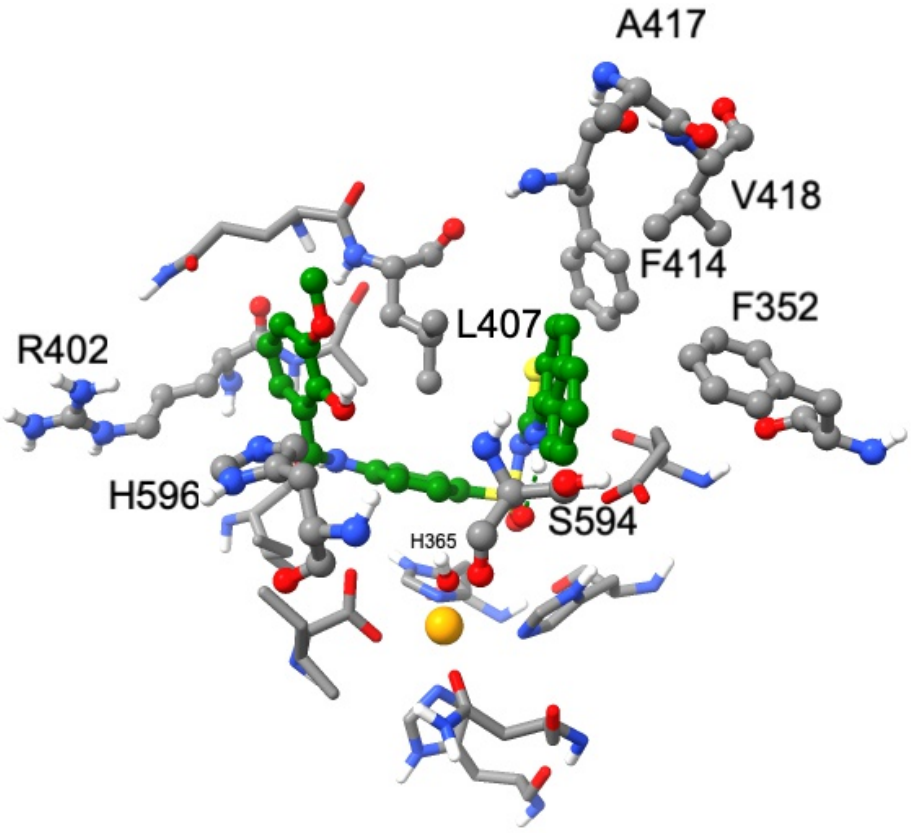

Figure 5. Predicted binding mode of **Lox12Slug001** with wt12-LOX. Residues that interact with the inhibitor are shown. Residues that mutated in the present study are shown in ball-and-stick representation and they are labelled. Carbon atoms of 12Slug001 are shown in green, whereas carbon atoms of wt12-LOX are shown in gray. Oxygen, nitrogen, hydrogen and sulfur atoms are shown in red, blue, white and yellow colors respectively. Fe^{3+} ion is shown as orange sphere. Hydroxide ion is shown in ball-and-stick representation.

When **Lox12Slug001** was screened against the A417I/V418M mutant, the potency decreased 2.4-fold, similar to that seen with **ML355**, indicating additional cavity area near the (naphthyl)thiazole moiety of **Lox12Slug001** (**Figure 6**). Previously, we observed with AA catalysis that to affect substrate binding, it was necessary to not only shorten the active site cavity (A417I/V418M) but to also make it narrower (S594T). The triple mutant, A417I/V418M/S594T, restricted the methyl tail of AA sufficiently to increase 15-HETE production significantly [32]. Therefore, we tested both **ML355** and **Lox12Slug001** against A417I/V418M/S594T and observed a dramatic decrease in potency for both inhibitors (greater than 20 μM IC_{50} values for both **ML355** and **Lox12Slug001** (**Table 3**)). These results indicate that by reducing both the active site depth and width, the inhibitor potency is reduced, supporting our inhibitor docking model.

As discussed above, L407 plays a role in **ML355** binding by interacting with its phenyl ring linker and positioning the ends of **ML355** properly in the "U" shaped cavity. It was therefore postulated that mutating L407 could have an additive effect with other mutants and thus the triple mutant, L407G/A417I/V418M, was designed to investigate the effect of both widening and reducing the length of the active site cavity on **ML355** positioning. This triple mutant lowered the inhibitor potency dramatically for both **ML355** and **Lox12Slug001** with IC_{50} values of >80 and >150 uM, respectively (**Table 3**), indicating that, without the bulk of L407, a more shallow active site impedes inhibitor binding. Finally, it should be noted that the IC_{50} value trend of **Lox12Slug001** against the mutants, A417I/418M, A417I/V418M/S594T and L407G/A417I/V418M (**Table 3**), are similar to the IC_{50} value trend of **ML355**, suggesting a similar binding mode between **Lox12Slug001** and **ML355**.

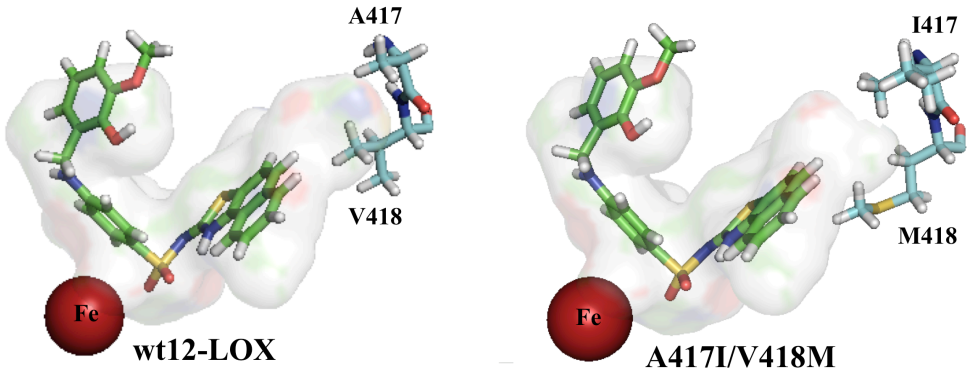

Figure 6. Relative cavity sizes of **Lox12Slug001** binding in the active site of **(A).** wt12-LOX and **(B).** A417I/V418M (Sloane determinants)

Enzyme	ML355 (μM)	Lox12Slug001 (μM)
wt12-LOX	0.36 ± 0.02	0.05 ± 0.02
A417I/V418M	0.83 ± 0.18	0.12 ± 0.04
A417I/V418M/S594T	>20 (45 % [a])	>20 (44 % [a])
L407G/A417I/V418M	>80 (19 % [a])	>150 (10 % [a])

Table 3. IC_{50} values of **(A). ML355** and **(B). Lox12Slug001** with wt12-LOX and the mutants of Sloane determinants. [a]Percent inhibition at 20 μM inhibitor.

Inhibitor	12-LOX (μM)	h5-LOX (μM)	h15-LOX-1 (μM)	h15-LOX-2 (μM)
Lox12Slug001	0.05 ± 0.02	>100	>100	>100

Table 4. IC_{50} values of **Lox12Slug001** for selected lipoxygenases.

3.4 π-π Interactions of ML355 and Lox12Slug001 with F352 and F414 12-LOX

The **ML355** docking model predicts that the benzothiazole ring of **ML355** is buried in a hydrophobic pocket created by the aromatic side chains of F352 and F414, with closest distances to **ML355** being 4.1 Å and 4.5 Å, respectively (**Figure 1**). Considering that **Lox12Slug001** appears to have a similar binding mode to **ML355** in the 12-LOX active site, we hypothesized that these aromatic residues could participate in π–π interactions with the benzothiazole moieties of both **ML355** and **Lox12Slug001** (**Figure 7**). Therefore, the mutants, F352L and F414L, were generated, however for **ML355**, only a modest increase in IC_{50} was observed, compared to wt12-LOX (**Table 5**). On the other hand, the IC_{50} values of **Lox12Slug001** against these mutants increased more significantly, with a 3.6-fold increase for F414L and a 9.8-fold increase for F352L (**Table 5**). These results are intriguing because both mutations increase the active site cavity size, but they have a greater negative effect on the larger inhibitor, **Lox12Slug001**. This suggests that there is a specific interaction with **Lox12Slug001** that is not present in **ML355**, which is disrupted upon the decreased size and loss of aromaticity in the active site mutations. Since **Lox12Slug001** is not only larger but has a more extensive aromatic structure than **ML355**, the data is consistent with **Lox12Slug001** having a stronger π–π interaction with F352 and F414 than **ML355**, which is lost upon mutation.

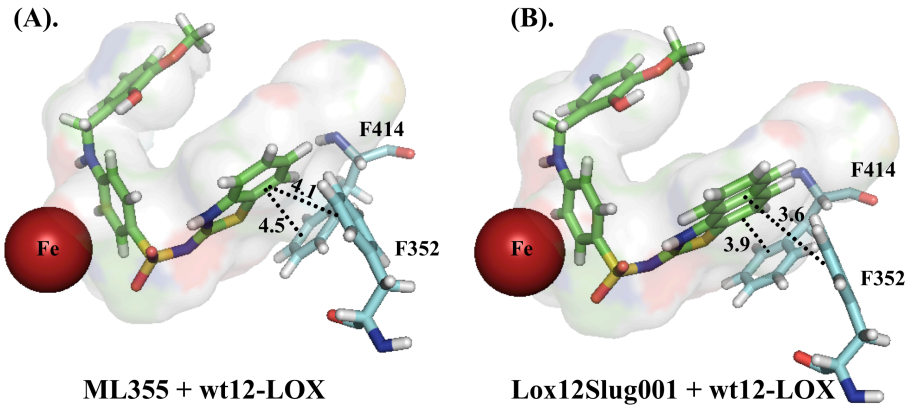

Figure 7. Predicted binding mode of **(A). ML355** and **(B). Lox12Slug001** in the active site of wt12-LOX showing the closest distances of benzothiazole ring to aromatic side chains of F352 and F414.

Enzyme	ML355 (μM)	Lox12Slug001 (μM)
wt12-LOX	0.36 ± 0.02	0.05 ± 0.02
F414L	0.49 ± 0.03	0.18 ± 0.01
F352L	0.89 ± 0.08	0.49 ± 0.05

Table 5. IC_{50} values of wt12-LOX, F414L and F352L with **ML355** and **Lox12Slug001** to investigate π–π interactions.

3.5 H596 binding Interaction with the p-methoxy catechol moiety of ML355

The role of R402 was previously determined to be unimportant with respect to substrate binding to 12-LOX [32] and in this work, R402 was also determined to not affect **ML355** binding (**Table 2**). However, computational prediction and subsequent experimental study showed that H596 did play a role in anchoring the carboxylate of AA during catalysis.[32] Considering this result and close proximity (3.6Å) of the H596 epsilon nitrogen (NE) to the oxygen atom of the hydroxyl group of p-methoxy catechol moiety of **ML355** (**Figure 8A**), H596L was generated and displayed a 5-fold decrease in potency relative to wt12-LOX, 1.8 ± 0.4 μM and 0.36 ± 0.02 μM, respectively (**Table 2**). These results suggest that H596 in 12-LOX may contribute to properly positioning **ML355** in the active site, possibly through the interaction with the p-methoxy phenol moiety of **ML355**, as observed in the docking model. Finally, it should be noted that an additional 7 mutations of active site residues were generated, but these did not significantly affect the potency of **ML355** and thus were not investigated further (Supporting Information, **Table S1**).

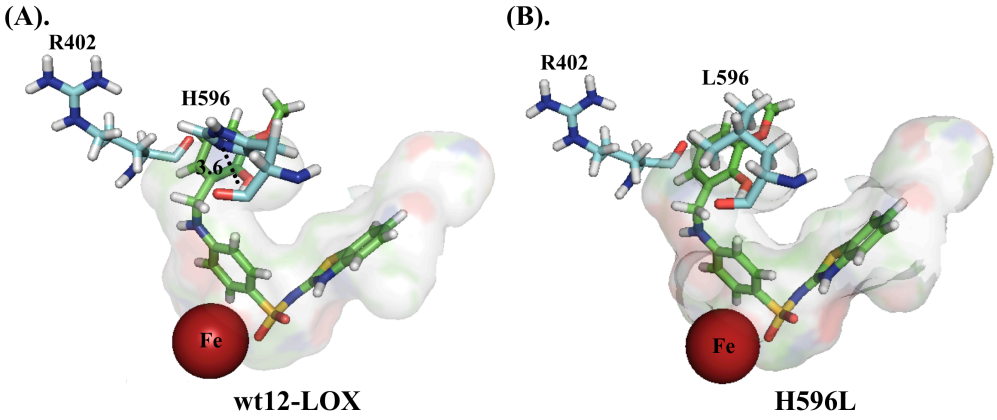

Figure 8. Predicted binding mode of ML355 in the active site of wt12-LOX interacting with **(A)** H596 and **(B)** H596L.

3.6 Islet Effect: Lox12Slug001 Improves GSIS and Increases Insulin Secretion of Human Islets Treated with PIC

Given the improved potency of **Lox12Slug001** against 12-LOX, its potency in islet cells was investigated. Glucose-stimulated insulin secretion (GSIS) of normal human and mouse islet cells, demonstrate increased insulin production, however, when exposed to pro-inflammatory cytokines (PIC), the difference between stimulated and unstimulated cells decreases. This exposure of PIC to both human and mouse β cells upregulates the 12-LOX pathway, and the inhibition of this 12-LOX pathway was implicated in protecting the viability and function of human and mouse β cells after PIC exposure.[5] Since **ML355** was previously shown to be a highly selective inhibitor of 12-LOX with a favorable ADME profile in protecting human islets against the impairment of GSIS by PIC [25], **Lox12Slug001** was also tested (**Figure 9**). As a control, human islet cells treated with 18 mmol/L of glucose (HG) showed a marked increase in insulin secretion (224+/-50 mU/L) relative to 3 mmol/L of glucose (LG) (24+/-4 mU/L). PIC treatment for 24 hrs increased basal insulin secretion at 3 mmol/L of glucose (189+/-54 mU/L) and led to the reduction of further increases in insulin secretion at 18 mmol/L of glucose (241+/-50 mU/L). When 1μM **Lox12Slug001** was added along with the PIC (for 24 hrs), the difference in insulin production was restored, 140+/-3 mU/L (LG) and 352+/-10 mU/L (HG). As a control, when only **Lox12Slug001 (**1 μM) was added, a similar insulin secretion increase to vehicle was observed, 25+/-5 mU/L (LG) and 128+/-13 mU/L (HG).

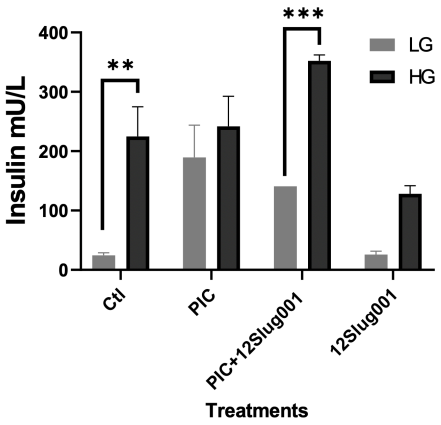

Figure 9. Batch incubation of human islets treated with PIC with or without the 12-LOX inhibitor, **Lox12Slug001**. GSIS was compared between human islets that were untreated (Ctl), pretreated with PIC, pretreated with PIC plus **Lox12Slug001** (1 μM) or pretreated with **Lox12Slug001** (1 μM) for 24 hours. Each condition from a single donor was performed in triplicate, and data from three donors were combined (n = 8 to 9). **P < 0.01;***P < 0.005 by Two-way Anova variance Sidak's multiple comparison test.

4. Conclusions

ML355 is a lead molecule targeting 12-LOX, a potential drug target to decrease platelet reactivity following vascular insult or injury.[26] Therefore, it is critical to investigate the binding mode of this promising lead molecule to its target in order to gain insights for further optimization. From the **ML355** docking pose in the 12-LOX active site, we mutated residues with the potential of affecting **ML355** binding and determined the **ML355** inhibitor potency against the mutants. These results were then compared to the calculated wt12-LOX/ **ML355**

binding affinities and the relationship between their docking score and inhibitor potency demonstrated a positive correlation, lending confidence to the docking model of **ML355** bound to the 12-LOX active site (**Figure 1**).

The docking model predicts a number of interactions between the active site and **ML355**. A key characteristic of the 12-LOX active site is its curved nature, which has been described as a "U" shape. L407 defines the "U" shape of the 12-LOX active site and has been shown to properly position the fatty acid, AA, for catalysis [32]. Appropriately, **ML355** conforms to the "U" shape of the 12-LOX active site, having specific interactions with active site residues. L407 is at the bottom of the "U", with **ML355** wrapping around the residue, with interaction to the phenyl linker region of **ML355**. Reducing the size of L407 progressively decreases **ML355** potency, manifesting a 7.2-fold decrease in the IC_{50} value with L407G (**Figure 3**), supporting the hypothesis that **ML355** gains binding affinity from the curvature of the active site.

Beyond L407, the benzothiazole of **ML355** extends into the bottom of the active site cavity, pointing towards the Sloane determinants, residues A417 and V418. However, the docking model indicates limited interaction between **ML355** and these residues. This lack of interaction was confirmed by the lack of effect by the cavity reducing mutation, A417I/V418M. This result indicated that a potential active site cavity was present such that the volume of **ML355** could be increased by attaching substituents to the benzothiazole moiety and thus optimize van der Waals interactions. In order to test this hypothesis, a derivative of **ML355** with a larger naphthyl-benzothiazole, **Lox12Slug001** (**Scheme 1**), was designed and shown to dock to the active site better than **ML355**. It was therefore synthesized and found to have 7.2-fold greater potency than **ML355** against 12-LOX (**Table 3**), supporting our docking model. Unexpectedly, the double mutant, A417I/V418M, only had a 2.4-fold increase in the IC_{50} with **Lox12Slug001**, suggesting additional cavity space even with **Lox12Slug001**. If, however, the cavity volume was also narrowed, A417I/V418M/S594T, the IC_{50} increased dramatically to greater than 20 uM, for both **ML355** and **Lox12Slug001** (**Table 3**). This result suggests that both the depth and width of the active site affect inhibitor binding. The specificity of the inhibitor/active site interaction was also confirmed with loss of inhibitor potency with the triple mutant, L407G/A417I/V418M (**Table 3**). The curious aspect of this mutation is that by increasing the size of the active site in the middle of the cavity, but reducing the size at the end of the cavity abolishes inhibitor potency, suggesting that both **ML355** and **Lox12Slug001** interact with L407 in such a way as optimize their active site binding.

Another aspect of the active site of 12-LOX is the aromaticity on key residues, F414 and F352, which the model suggests interacts with the aromatic moieties of the inhibitors (**Figure 7**). However, loss of the aromaticity of F414 and F352 affected the potency of **Lox12Slug001** more so than **ML355**. This suggests a difference in their binding mode, with **Lox12Slug001** potentially having more pi-pi interactions with F414 and F352 than **ML355**. This is a reasonable hypothesis since **Lox12Slug001** has a more extensive pi-system than **ML355**.

Computational prediction and subsequent experimental study showed that H596 could play a role in anchoring the carboxylate of AA during catalysis but not R402[26]. Therefore, both H596 and R402 were replaced with a nonpolar leucine and the inhibitory potency against **ML355** was tested. H596L showed a greater increase in the IC_{50} than that of R402 relative to wt12-LOX (5-fold increase for H596L and 0.8-fold for R402L), suggesting that H596 in 12-LOX may contribute to properly positioning **ML355** binding in the active site but not R402, possibly through the interaction with the p-methoxy phenol moiety of **ML355** (**Table 2**).

The gain in potency of **Lox12Slug001** supported our binding hypothesis however, its improved potency also suggested improved drug qualities. Gratifyingly, its selectivity against other LOX isozymes was maintained (**Table 4**) and more importantly, it maintained its potency in PIC challenged human islet cells, comparable to that of **ML355** [25] (**Figure 9**). These results are supportive of **Lox12Slug001** being an effective drug candidate for platelet ailments and diabetes. Further studies are currently being pursued to derivatize **ML355** in order to optimize the additional space in the active site and develop them as a potential diabetes therapeutics.

Acknowledgements

The authors would gratefully like to acknowledge the NIH funding (TRH (AG047986) and JLN (DK105588)) and Dr. Diane Luci and the NCGC for the synthesis of **ML355** and helpful discussions. The authors are also thankful to Gabriella Alvarez for helping with various experiments. Human Islets were provided to JLN through the Human Islet Distribution Program (IIDP). M.P.J. is a consultant to Schrodinger Inc., which provided some of the software used in this work.

Graphic for the table of contents

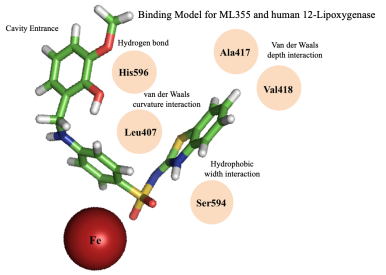

References

1. Brash, A.R., *Lipoxygenases: Occurrence, Functions, Catalysis and Acquisition of Substrate.* J. Biol. Chem., 1999. **274**(34): p. 23679-23682.
2. Kuhn, H., et al., *Structural biology of mammalian lipoxygenases: enzymatic consequences of targeted alterations of the protein structure.* Biochem Biophys Res Commun, 2005. **338**(1): p. 93-101.
3. Pidgeon, G.P., et al., *Lipoxygenase metabolism: roles in tumor progression and survival.* Cancer Metastasis Rev, 2007. **26**(3-4): p. 503-24.
4. Burkhart, J.M., et al., *The first comprehensive and quantitative analysis of human platelet protein composition allows the comparative analysis of structural and functional pathways.* Blood, 2012. **120**(15): p. e73-82.
5. Dobrian, A.D., et al., *Role of the 12-lipoxygenase pathway in diabetes pathogenesis and complications.* Pharmacol Ther, 2019. **195**: p. 100-110.
6. Yeung, J., et al., *12-lipoxygenase activity plays an important role in PAR4 and GPVI-mediated platelet reactivity.* Thromb Haemost, 2013. **110**(3): p. 569-81.
7. Ciko, Z., *[Circulating platelet aggregation in ischemic heart disease].* Vojnosanitetski pregled. Military-medical and pharmaceutical review, 1981. **38**(1): p. 17-9.
8. Chen, S.H., *[Observations on platelet aggregation in patients with ischemic heart disease].* Zhonghua yi xue za zhi, 1985. **65**(7): p. 414-7.
9. Dreyfuss, F. and J. Zahavi, *Adenosine diphosphate induced platelet aggregation in myocardial infarction and ischemic heart disease.* Atherosclerosis, 1973. **17**(1): p. 107-20.
10. Elwood, P.C., et al., *Ischemic heart disease and platelet aggregation. The Caerphilly Collaborative Heart Disease Study.* Circulation, 1991. **83**(1): p. 38-44.
11. Gormsen, J., et al., *ADP-induced platelet aggregation in vitro in patients with ischemic heart disease and peripheral thromboatherosclerosis.* Acta medica Scandinavica, 1977. **201**(6): p. 509-13.
12. Gryglik, J., *[Pharmacological inhibition of platelet aggregation in primary and secondary prevention of ischemic heart disease].* Polski tygodnik lekarski, 1979. **34**(13): p. 509-11.
13. Helo, O.H., J.K. Madsen, and J. Kastrup, *[Treatment of ischemic heart disease with the platelet aggregation inhibitor clopidogrel].* Ugeskrift for laeger, 2004. **166**(18): p. 1659-62.
14. Yeung, J. and M. Holinstat, *Newer agents in antiplatelet therapy: a review.* J Blood Med, 2012. **3**: p. 33-42.
15. McMahon, G.S., et al., *Transient heparin-induced platelet activation linked to generation of platelet 12-lipoxygenase. Findings from a randomised controlled trial.* Thromb Haemost, 2013. **109**(6): p. 1099-107.
16. Svensson Holm, A.C., et al., *Inhibition of 12-lipoxygenase reduces platelet activation and prevents their mitogenic function.* Platelets, 2014. **25**(2): p. 111-7.
17. Suzuki, H., et al., *Hinokitiol, a selective inhibitor of the platelet-type isozyme of arachidonate 12-lipoxygenase.* Biochemical and Biophysical Research Communications, 2000. **275**(3): p. 885-889.

18. Segraves, E.N., et al., *Probing the activity differences of simple and complex brominated aryl compounds against 15-soybean, 15-human, and 12-human lipoxygenase.* J Med Chem, 2004. **47**(16): p. 4060-5.
19. Vasquez-Martinez, Y., et al., *Structure-activity relationship studies of flavonoids as potent inhibitors of human platelet 12-hLO, reticulocyte 15-hLO-1, and prostate epithelial 15-hLO-2.* Bioorganic & Medicinal Chemistry, 2007. **15**(23): p. 7408-25.
20. Deschamps, J.D., et al., *Discovery of platelet-type 12-human lipoxygenase selective inhibitors by high-throughput screening of structurally diverse libraries.* Bioorganic & Medicinal Chemistry, 2007. **15**(22): p. 6900-8.
21. Kenyon, V., et al., *Discovery of potent and selective inhibitors of human platelet-type 12-lipoxygenase.* J Med Chem, 2011. **54**(15): p. 5485-97.
22. Luci, D.K., et al., *Synthesis and Structure-Activity Relationship Studies of 4-((2-Hydroxy-3-methoxybenzyl)amino)benzenesulfonamide Derivatives as Potent and Selective Inhibitors of 12-Lipoxygenase.* J Med Chem, 2014. **57**(2): p. 495-506.
23. Yeung, J., et al., *Platelet 12-LOX is essential for FcgammaRIIa-mediated platelet activation.* Blood, 2014. **124**(14): p. 2271-9.
24. Adili, R., et al., *First Selective 12-LOX Inhibitor, ML355, Impairs Thrombus Formation and Vessel Occlusion In Vivo With Minimal Effects on Hemostasis.* Arterioscler Thromb Vasc Biol, 2017. **37**(10): p. 1828-1839.
25. Ma, K., et al., *12-Lipoxygenase Inhibitor Improves Functions of Cytokine-Treated Human Islets and Type 2 Diabetic Islets.* J Clin Endocrinol Metab, 2017. **102**(8): p. 2789-2797.
26. Tourdot, B.E. and M. Holinstat, *Targeting 12-Lipoxygenase as a Potential Novel Antiplatelet Therapy.* Trends Pharmacol Sci, 2017. **38**(11): p. 1006-1015.
27. Andreou, A. and I. Feussner, *Lipoxygenases - Structure and reaction mechanism.* Phytochemistry, 2009. **70**(13-14): p. 1504-10.
28. Amagata, T., et al., *Exploring sponge-derived terpenoids for their potency and selectivity against 12-human, 15-human, and 15-soybean lipoxygenases.* J Nat Prod, 2003. **66**(2): p. 230-5.
29. Robinson, S.J., et al., *Using enzyme assays to evaluate the structure and bioactivity of sponge-derived meroterpenes.* Journal of Natural Products, 2009. **72**(10): p. 1857-63.
30. Jameson, J.B., 2nd, et al., *A high throughput screen identifies potent and selective inhibitors to human epithelial 15-lipoxygenase-2.* PLoS One, 2014. **9**(8): p. e104094.
31. Smyrniotis, C.J., et al., *ATP allosterically activates the human 5-lipoxygenase molecular mechanism of arachidonic acid and 5(S)-hydroperoxy-6(E),8(Z),11(Z),14(Z)-eicosatetraenoic acid.* Biochemistry, 2014. **53**(27): p. 4407-19.
32. Aleem, A.M., et al., *Probing the Electrostatic and Steric Requirements for Substrate Binding in Human Platelet-Type 12-Lipoxygenase.* Biochemistry, 2019. **58**(6): p. 848-857.